Infiltration and Surface Geometry Features of a Swelling Soil following Successive Simulated Rainstorms

R. R. Wells, D. A. DiCarlo, T. S. Steenhuis,* J.-Y. Parlange, M. J. M. Römkens, and S. N. Prasad

ABSTRACT

The theory of water movement in high shrink/swell soils has experienced consistent revision since Haines first presented the topic in 1923. Several aspects of the infiltration process in cracking soils have proven to be difficult to measure; seal/crust formation and properties, crack network patterns, preferential flow zones and contributions, and soil moisture determinations within the profile (near crack and near center of prismatic column) to name a few. Here, we used simulated rainstorms, laser measurements of surface elevation, needle-penetrometer measurements, and mass measurements of infiltrating water over a 206- and 145-d period to examine water movement and cracking patterns in a large sample box filled with a swelling clay soil. Water movement was restricted to the neighborhood of the crack zone, since the formation of a surface seal/crust prohibited infiltration into the surface of the prismatic columns of soil between cracks. Also, the location of cracks was observed to alternate between rainstorms. The alternating crack pattern led to more uniform wetting with depth as time increased and the number of rainstorms increased, thereby reducing the extent of preferential flow.

Most of our understanding of infiltration and redistribution of water in soils comes from experiments with 'ideal' soils and models that depict the solid part of the soil as a rigid medium through which water passes. This may be an accurate assumption for stable uniformly structured soils with low clay content, but for many soils, the physical changes that take place (such as swelling, sealing, shrinkage, and cracking) during and after the rainstorm greatly affect the movement of water in the soil. In particular, in vertisols where large cracks form after drying, the cracks are zones of preferential transmission for water. Smiles (1974), drawing from Philip (1969), found that infiltration in swelling soils is very different from infiltration in rigid soils. Smiles (1974) found that infiltration was primarily a sorption phenomenon. Infiltration through the cracks leads to a non-uniform profile of water content, which affects the subsequent swelling and cracking of the soil. The interrelationship between these two processes is not catered for by traditional one- or two-dimensional models.

Using field observations, White (1970, 1972, 2001) presented a holistic model of how cracking soils develop and water infiltrates from one event to the next. He pointed to a moisture dependency that defines the arrangement and distribution of the cracks. Moreover, White (1972) explained the energy implications that cause the cracks to reappear in the same position from event to event. Johnston and Hill (1944) observed that cracks develop between crop rows where the water content was higher (due to less uptake by plants) and, thus, the strength of the soil was lower. Since dry clay soils tend to moisten more rapidly to a greater depth along a crack than at a distance from a crack, cracks transmit more water deeper under heavy precipitation events, making the soil wetter in this area.

Other authors have looked at cracking soils in the field. Dasog et al. (1988), using methods outlined by El Abedine and Robinson (1971), measured field crack networks and reported that moisture and swelling potential coupled with vegetation and management activities influence cracking. Waller and Wallender (1993) used image analysis of soil surface photographs to quantify prismatic column surface geometry, and noted that after irrigation the major cracks reformed in the same location. Chertkov and Ravina (1998) and Chertkov (2000) used the similarity between cracks in rocks and swelling clay soils to model crack network geometries in swelling clay soils. Bronswijk (1991) linked water content changes and easily measured physical properties of soil aggregates with shrinkage prediction and discussed a second normal shrinkage phase.

In addition to swelling and cracking, clay soils form a surface seal, which also greatly affects infiltration. Surface sealing occurs due to the impact of raindrops on the surface of the soil, causing compaction, and settling of fine-grained detached material on the surface of the soil, effectively clogging the micropores. The surface seal is thin, in comparison to the bulk material; however, the surface seal and bulk material exhibit very different infiltration characteristics. Tackett and Pearson (1965) used resistance methods to examine crust strength at various stages of simulated rainfall and concluded that resistance increased rapidly with small additions of clay. Mualem and Assouline (1989) presented a conceptual model of soil sealing, which described the seal as a non-uniform disturbed layer defined by minor differences in soil structure. Parlange et al. (1984), Baumhardt et al. (1990), Philip (1998), and Smith et al. (1999) discussed the theoretical aspects of infiltration into soils with a surface crust.

Most of the studies that have been performed in swelling soils have focused on crack pattern formation, surface seals, or infiltration; very few studies have looked at the interrelationships between these processes. The objective of this research was to study the processes that govern the relationship between cracks, surface seals, and infiltration in a highly swelling soil. We measured total infiltration and surface runoff in a packed

R.R. Wells, D.A. DiCarlo, and M.J.M. Römkens, USDA-ARS National Sedimentation Lab., Oxford, MS 38655; T.S. Steenhuis, and J.-Y. Parlange, Dep. of Biological and Environmental Engineering, Cornell Univ., Ithaca, NY 14853; S.N. Prasad, Dep. of Civil Engineering, Univ. of Mississippi, Oxford, MS 38677. Received 30 May 2002. *Corresponding author (tss1@cornell.edu).

Published in Soil Sci. Soc. Am. J. 67:1344–1351 (2003).

677 S. Segoe Rd., Madison, WI 53711 USA

clay soil box, where water was applied at a uniform rate using a rain simulator. Surface microrelief mapping was used before and after each rainstorm to observe the changes in the cracking pattern and the surface elevation from event to event. Also, the depth of the wetting front in the soil was measured at various positions using a specialized cone penetrometer. The results show that infiltration increased for the first four rainstorms, as the cracks develop deeper and transmit water to lower depths within the profile. Surprisingly, the surface cracks were not observed to return to the same position after each rainstorm, but cycled between locations every other rainstorm.

MATERIALS AND METHODS

Cracking Test Soil

Soil from 0- to 30-cm depth of a Sharkey clay (very-fine, smectitic, thermic Chromic Epiaquerts) from the Hester farm in Bolivar County, MS (Grid 87, 1958 USDA Soil Survey), was brought to the USDA-ARS National Sedimentation Laboratory, air-dried, and crushed to pass through a 2-mm sieve. Soil texture was determined to be 65% clay, 32% silt, and 3% sand. An X-ray analysis of a random soil sample revealed smectite as the dominant clay mineral.

Large Soil Box

A Plexiglas box (76.5 by 80 by 30 cm) was designed with a drain pan on the lower slope and a drainage system in the bottom of the box. The drainage system was covered and packed with five uniform layers of fine sand, each 1.6-cm layer consisting of 6.8 kg of sand. Soil was uniformly packed above the fine sand in 22 layers, each 1-cm layer consisted of 11.3 kg of soil (soil pack density of 1.4 g cm^{-3}). The soil sample was placed on a 2% slope and subjected to 3 h long rainstorms of 30 mm h^{-1} intensity. Two types of drying were used after the rainstorm: passive and aggressive. Passive drying (the sample was left alone at room temperature) occurred for a period of 48 h after the cessation of the rainstorm. Aggressive drying (the drying rate of the sample was accelerated with a fan blowing heated air over the surface) followed the passive drying and ended 12 h before the next rainstorm. Drying ceased when 90% of the total input for each rainstorm had evaporated. The fan was a 32.5-cm diameter household fan with three-speed control, positioned 2 m away and 20 cm above the upper slope of the sample, and the air was heated with five 250 W heat lamps, positioned 61 cm behind the fan. The lag of 48 h between the cessation of the rainstorm and the increase in drying power was used in the experiments to allow the crack network to establish a pattern, unaltered by blowing heated air across the surface.

Rainfall Simulator

A rainfall simulator was used to distribute the water to the soil sample. Meyer (1958) discussed similar laboratory equipment and gave a detailed analysis of the drop size produced from various nozzles, height specifications, and energy relations, compared with natural rainstorms. Our setup included an 80 to 150 nozzle centered 3 m above the soil surface, constant rainfall intensity (30 mm h^{-1}), and a constant duration (3 h).

Laser Profile Meter

A non-contact type infrared laser profile meter was used to determine the vertical surface elevation coordinate of the soil before and after each rainstorm event. The surface profilemeter utilized the principle of triangulation for distance measurements of reflected light from the soil surface to the gauge-probe sensor and was positioned above the surface, using an *x-y* stage. Römkens et al. (1986a, 1988) discuss similar systems and provide further technical information on performance aspects.

In the large sample box investigations, *x*-direction transects (perpendicular to the slope) of the surface elevation measurement were taken at a sampling interval of 0.1 cm. The *x*-direction transects were separated by 0.1 cm in the *y*-direction (parallel to the slope) within the flume. Surface elevation matrices were collected before, immediately following, and every 24 h after the rainstorm. The data presented in the surface elevation profile maps were collected as a matrix (725 × 734) of elevation measurements from the soil sample (total sampled length of 72.5 cm in the *x*-direction and 73.4 cm in the *y*-direction).

A limitation of the laser system was the configuration of the light source and sensor. The angle and distance of the sensor from the light source created gaps in the data in the neighborhood of the crack. The surface features were clear, but the subsurface features were dependent on the position of the sensor in relation to the crack face and tip. When the gauge-probe and subsurface crack features were parallel, the elevation observations were reliable. When the gauge-probe and subsurface features were perpendicular, the reflected light from the subsurface evaded the sensor, thereby resulting in an invalid measurement being recorded into the data file. The data recorded during invalid observations were synonymous with the most recently recorded valid observation. The invalid measurements were continually recorded until the sensor detected the reflected light from the sample. However, before the formation of deep surface cracks, the laser system produced no erroneous points. The laser system gave accurate surface elevation measurements on the opening of the cracks, although there were serious elevation inaccuracies within the openings. When needed, accurate crack depths were measured manually.

Needle Penetrometer

A needle penetrometer was manufactured to measure the depth of the wetting front along a single transect of the soil, immediately after each rainstorm. The apparatus consisted of an aluminum rectangular channel, a needle penetrometer, and a 500-g weight. The channel was positioned parallel to the surface drain and perpendicular to the surface slope. Holes, slightly larger than the base area of the cone on the needle penetrometer, were drilled at 1.27-cm intervals along the centerline of the channel and leveling feet were mounted to either end of the channel. The 60° cone (total included angles at the penetrometer tip) of the needle penetrometer was machined from oil-hardened tool steel and the shaft consisted of a stainless steel Becton-Dickinson YALE hypodermic needle (13G2 Short Bevel, BD Biosciences, Franklin Lakes, NJ) and a 0.0016-cm drill bit. Depth measurements of the wetting front were obtained by measuring the depth of penetration of the needle with the 500-g weight placed on top. We found by trial and error that by using the 500-g weight, immediately after the rainstorm, the needle penetrated through the wet soil, but not the dry soil.

Table 1. The physical surface data were measured in Exp. A and the penetration depths in Exp.B. The mean prism dimension and mean crack depths and widths were measured after the drying time shown, and provide the initial condition for the subsequent rainstorm. The minimums and maximums are provided in parenthesis.

			Exp. A		
Rainstorm cycle number	Cumulative infiltration	Drying time	Prism dimension	Crack depth	Crack width
	mm	d	cm		
1	9.5	9	10 (8.7, 11)	3 (2.6, 3.1)	1.3 (0.9, 1.6)
2	14.2	21	9.9 (8, 12.2)	5.2 (5, 5.5)	1.3 (0.8, 1.6)
3	19.4	21	8.9 (6.4, 11.5)	7 (4.8, 8.3)	1.2 (0.7, 1.7)
4	23.1	24	10 (8, 11.6)	6.5 (5.8, 7.2)	1.4 (1, 2)
5	18.5	87	10.7 (8.5, 13)	8.3 (5, 12)	1.4 (0.6, 2)
6	15	31	11.5 (9, 16)	9 (6.2, 12.7)	1.3 (1, 1.6)
7	20.4	13	11.9 (7.5, 18)	9.2 (7, 14)	1.4 (0.8, 1.8)
8	14.9				

		Exp. B	
Rainstorm cycle number	Cumulative infiltration	Drying time	Maximum penetration depth
	mm	d	cm
1	n.a.	8	3
2	14.3	17	5.5
3	16.5	58	8
4	17.4	62	9.5
5	23.5		

Infiltration Balance

The cumulative infiltration measurements were obtained from a load cell placed beneath the sample box. The balance was a Fairbanks model H90-5150 (Fairbanks Scales, Kansas City, MO) with a 450-kg capacity and a resolution of 0.05 kg. The balance readings were recorded on a 10-s interval during the rainstorm, 10-min intervals for 24 h following the rainstorm, and then all subsequent readings were recorded at 1-h intervals.

Sediment Concentration

The sediment concentration measurements were obtained by catching water and sediment running off the drain pan at regularly spaced time intervals. The runoff sample was weighed, a coagulation reagent was added to settle the soil, then the water was removed, and the remaining soil dried in an oven at 105°F for 24 h. The resulting dried soil sample was weighed to determine the sediment concentration of the runoff sample per unit water running off the soil sample per unit time.

RESULTS

Two experiments were performed sequentially in the same box, hereafter referred to as Exp. A and Exp. B. Crack network pattern development was the same between the two experiments. The experiment schedule, containing information about the rainstorms and drying periods, is provided in Table 1. Similar results were obtained in both experiments; however, the needle penetrometer hole left after penetration created a distinct disruption of the crack network (in the neighborhood of the penetrometer hole); therefore, we present the laser profile data, cumulative infiltration data, sediment concentration data, and soil heave calculations from Exp. A and the needle penetrometer measurements from Exp. B. In addition, several other smaller soil boxes showed qualitatively the same results, but the crack network was affected by the finite size of the smaller boxes. Although the procedure of water application and drying were exactly the same between the two experiments, to keep the water balance equal, different drying times were needed, most likely due to environmental (ambient humidity, etc.) conditions.

We present the results of each storm in chronological order. During the first rainstorm in both experiments, runoff began 4 min into the rainstorm. The sediment concentration varied from a maximum of 11.3 mg L^{-1} (12 min into the rainstorm), declining to 0.8 mg L^{-1} near the end of the rainstorm. Soil swelling was observed almost immediately after the rainstorm began and continually modified the soil throughout the rainstorm. The cumulative infiltration (Table 1) for this and all subsequent rainstorms for Exp. A showed a steady increase through four rainstorms then declined for the fifth and sixth rainstorms.

Penetration measurements, taken in Exp. B immediately after the first rainstorm, are shown in Fig. 1A. The wetting front is linear and reaches a depth of approximately 3 cm, which is consistent with wetting observations along the sidewalls of the Plexiglas box. The surface elevation measurements in Exp. A immediately following the first rainstorm are shown in Fig. 2. The color scale is reduced in this figure to magnify surface features discussed later in this paper.

The soil surface elevation measurements, after 9 d of drying, in Exp. A are shown in Fig. 3. The soil cracked into prismatic columns (10 cm average dimension). The crack depths in Fig. 3 are cut off at the original soil height of 0.00 cm, since the profile meter cannot accurately measure the depths of the bottom of the crack. Crack depth and width, taken with a semi-rigid plastic stick, are shown in Table 1. The surface of each prismatic column is bowl shaped, with the lowest elevation in the center radiating out to the highest elevation near the edges (Fig. 3).

During the second rainstorm, we observed in both experiments increased initial infiltration followed by ponding of water within the bowls (Fig. 3). The water then ran out of the bowls and into the cracks. Also, some of the edges of the columns sloughed off into the

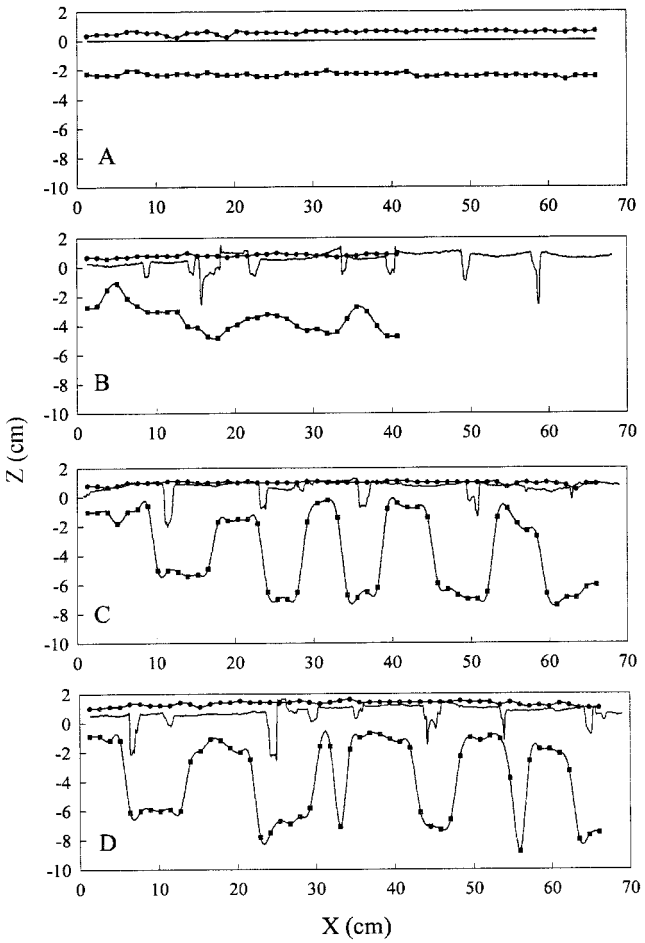

Fig. 1. The solid line represents the laser elevation of the soil surface before the rainstorm, the circular symbols represent the elevation of the soil surface immediately after the rainstorm, before penetration, and the diamond symbols represent the final position of the penetrometer immediately after the rainstorm, after application of the 500-g load. (A) Needle penetration measurements from Exp. B, immediately following the first rainstorm. (B) Immediately following the second rainstorm. (C) Immediately following the third rainstorm. Here, the depth of the wetting front, near the column centers, is less than the previous rainstorm, while the depth of wetting near the previous cracks is greater. (D) Immediately following the fourth rainstorm. The depth of wetting near the previous cracks increased 2 cm, while the depth of wetting near the previous prismatic column centers remained 2 cm below the surface. (Cracks formed after the first rainstorm and following each subsequent rainstorm.)

cracks. Runoff in both experiments commenced 14 min after the onset of the rainstorm when most of the cracks had filled with water, but before the cracks swelled close. The sediment concentration varied from a maximum of 3.8 mg L^{-1} (25 min into the rainstorm), declining to 0.8 mg L^{-1} near the end of the rainstorm. The cumulative infiltration for this rainstorm in Exp. A is presented in Table 1. We see a doubling of the total infiltration compared with the previous rainstorm where there were no cracks.

Penetration measurements, taken in Exp. B immediately following the second rainstorm, are shown in Fig. 1B. The wetting front is clearly non-uniform and, in the neighborhood of the previous crack, the penetration depth is 5.5 cm compared with the initial penetration depth (Fig. 1A) of 3 cm. This is consistent with our visual observations of greater water infiltration in and around the cracks.

Figure 4 shows the soil surface elevation after 21 d of drying in Exp. A after the second rainstorm. In Fig. 4, notice that the centers of the previous prismatic columns (Fig. 3) have become the corners of the present prismatic columns and the corners are now the centers. We also notice in several cases that the center, 2 to 3 cm of the previous prismatic columns, have become much smaller prismatic columns with cracks radiating from them. For example, in Fig. 4 at 64 cm on the *x*-axis there are three of these features located at 40, 50, and 60 cm.

In the third rainstorm, water movement observations were similar within the sample as the second rainstorm in both experiments. The cumulative infiltration (Table 1) nearly tripled that of the first rainstorm in Exp. A. Penetration measurements, taken in Exp. B immediately after the third rainstorm, are shown in Fig. 1C. The depth of the wetting front in the neighborhood of the previous cracks increased from 2.5 to 8 cm, but in the neighborhood of the previous prismatic column center the wetting front decreased by 1 to 2 cm, as compared with the initial rainstorm event wetting front depth of 3 cm.

Figure 5 shows the soil surface elevation after 21 d of drying in Exp. A after the third rainstorm. In Fig. 5, the soil surface reverted back to the initial cracking pattern (Fig. 3), although some of the smaller prismatic columns present in the initial cracking pattern coalesced with their nearest neighbor forming larger prismatic columns.

In the fourth rainstorm, water movement observations were similar to the second and third rainstorms in both experiments. Penetration measurements, taken in Exp. B immediately after the rainstorm, are shown in Fig. 1D. The depth of the wetting front in the neighborhood of the previous cracks was similar to the result shown in Fig. 1C. The penetration measurements near the previous cracks increased 1.5 cm and near the previous column centers the depth stabilized at 2 cm. Figure 6 shows the soil surface elevation after 24 d of drying. The corners of the former columns coalesced to form the centers of new prismatic columns and vice-versa. Subsequent rainstorms showed the same qualitative behavior and a summary of the surface features are in Table 1.

By comparing initial surface elevation measurements with subsequent surface elevation measurements, soil heave estimates were quantitatively made. Individual surface transects were integrated and multiplied by the laser spot size (0.008 cm^2) to yield a slice volume measurement. The slice volume measurements were summed to obtain a total sample volume measurement. The increase in sample height was obtained by subtracting the initial sample volume from all subsequent sample volumes then dividing by the area of the sample. In Fig. 7, there are sharp increases in the total sample height on the days of the rainstorm and slow declines during evaporation. We also notice that the sample height continues to increase for 2 to 3 d following the rainstorm as much

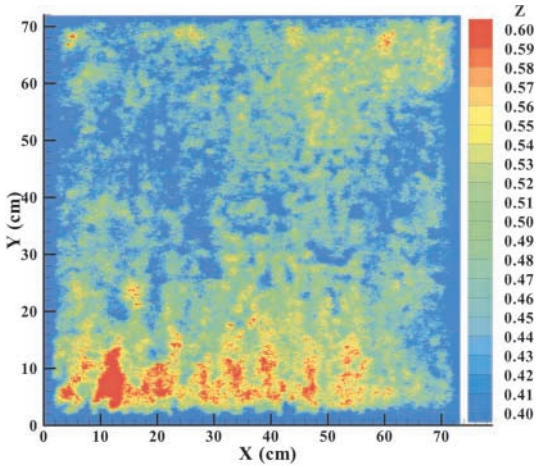

Fig. 2. Surface elevation map from Exp. A, immediately following the first rainstorm. The surface elevations are presented in centimeters, with the hot colors denoting the highest elevations.

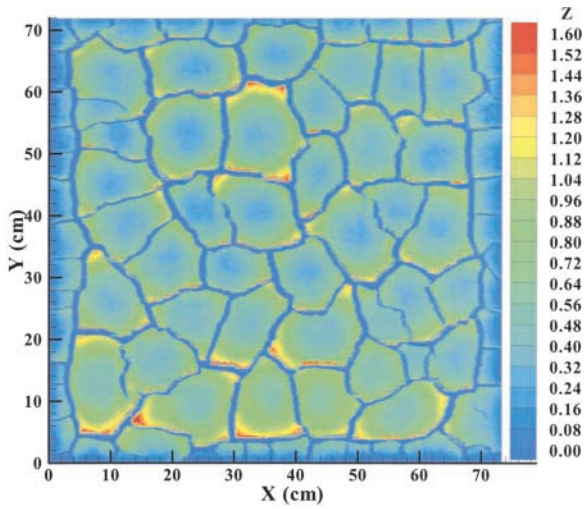

Fig. 3. Surface elevation map from Exp. A, following the first rainstorm, after 9 d of drying. The surface elevations are presented in centimeters, with the hot colors denoting the highest elevations. Each prismatic column surface resembles a bowl, with higher elevations radiating away from the center of the column.

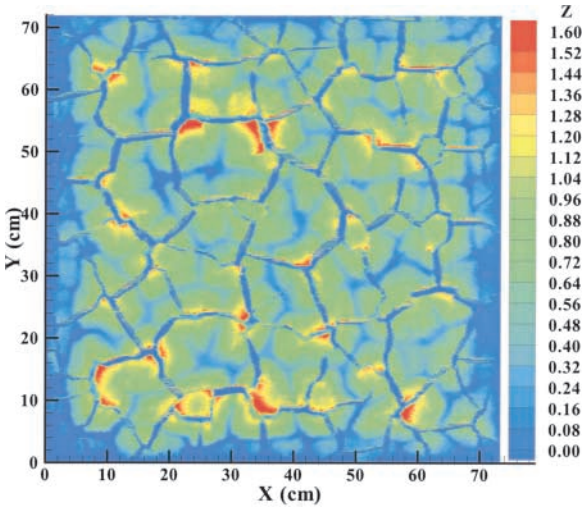

Fig. 4. Surface elevation map from Exp. A, following the second rainstorm, after 21 d of drying. The surface elevations are presented in centimeters, with the hot colors denoting the highest elevations. Previous cracks (Fig. 3) are now the lowest elevations and vice-versa. In several cases, the centers of the previous prismatic columns formed reduced columns with cracks branching out.

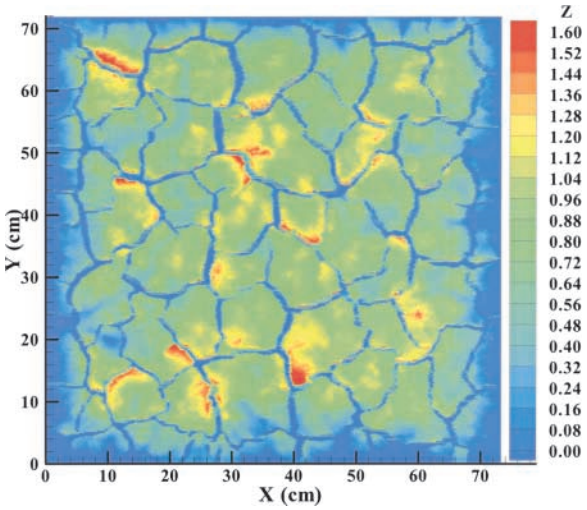

Fig. 5. Surface elevation map from Exp. A, following the third rainstorm, after 21 d of drying. The cracking pattern is similar to the pattern in Fig. 3, but the bowl shape is not obvious.

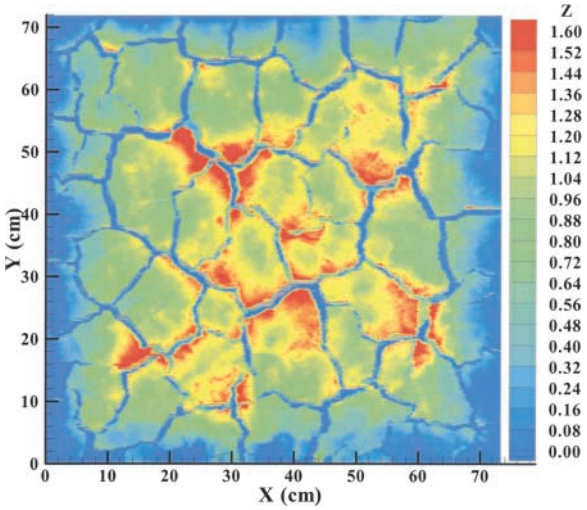

Fig. 6. Surface elevation map from Exp. A, following the fourth rainstorm, after 24 d of drying. The prismatic column size increased to 10 cm, but the position of the prismatic columns and the cracking pattern is similar to Fig. 4.

as 0.2 cm. This is interesting in the fact that the total volume of the soil was increasing even though the water contained within the soil was decreasing. The decrease in height only began after the soil started cracking.

DISCUSSION

The sum of the needle penetrometer, cumulative infiltration, and surface elevation results yield interesting insights on how the distribution of water within the soil profile affects the formation of cracks which, in turn, affects the subsequent cumulative infiltration, subse-

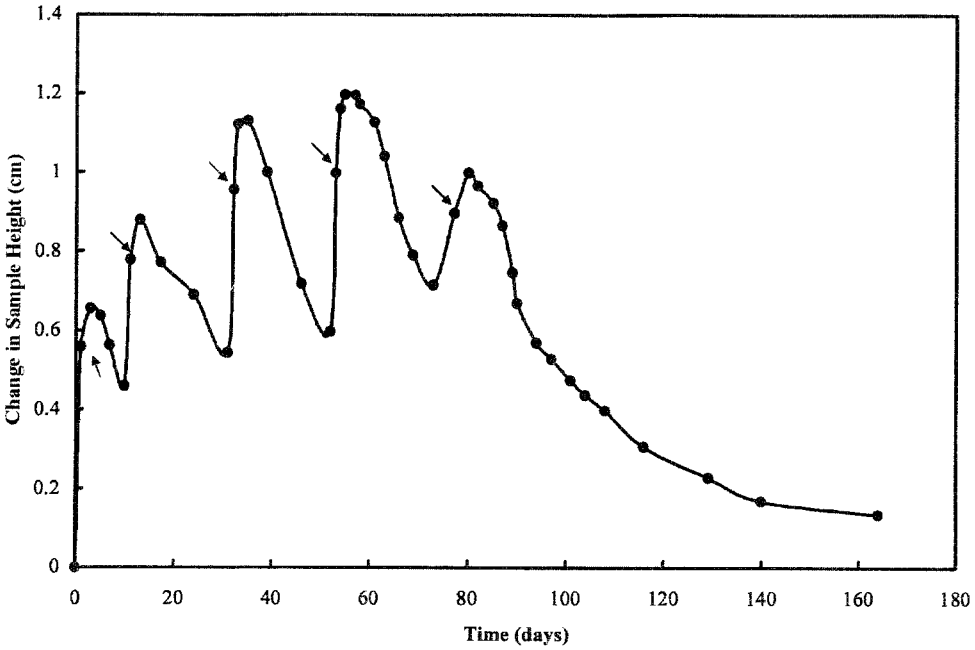

Fig. 7. Soil heave estimates from Exp. A through five rainstorms and five drying periods, calculated from the surface elevation measurements by subtracting the initial dry pack sample elevation measurements from subsequent sample elevation measurements. The arrows point to the heave estimates immediately following the rainstorm.

quent distribution of water within the soil profile, and crack patterns.

The observations and measurements of infiltration and runoff during and immediately after rainfall are straightforward. Due to the low permeability of the surface seal and high transmissivity of the cracks, almost all of the water infiltrates through the surface cracks. The infiltration rate at the surface of the prismatic column is hindered by the presence of the surface crust, derived from the kinetic energy of the rainstorm and the deposition of dispersed soil particles (Römkens et al., 1986b; Bonsu, 1992). The water entering the crack space initiates lateral infiltration into the walls of the prismatic columns and vertical infiltration into as yet unwetted aggregates (Germann and Beven, 1982). As the rainstorm continues, the prismatic columns coalesce through swelling and sloughing to close the cracks. At this time, little to no water infiltrates from the surface of the prismatic columns and infiltration through the former cracks is reduced, in part, through seal formation.

The cumulative infiltration measurements provided in Table 1 for Exp. A show that the total amount of water infiltrating into the soil increases as the number of rainstorms increases, up until the fifth rainstorm. The cumulative infiltration in the fifth rainstorm dropped, most likely, because the drying time was less than the previous drying time and the sample was not allowed to fully dry. The same is true for the seventh and eighth rainstorms. Figure 8 presents the cumulative infiltration versus the average crack depth for all rainstorms. The average crack depth measurements, obtained before the rainstorm, were paired with subsequent cumulative infiltration amounts. These results show a linear increase in the cumulative infiltration as the average crack depth increases for the first four rainstorms. This agrees with the assumption that most water infiltrates into the crack network. With greater crack depth, there is greater surface area for greater infiltration. Surprisingly, this linear relationship breaks down for the fifth and subsequent rainstorms. This may be partially due to the drying time being less between some of the later rainstorms, but we do not find a solid dependence of infiltration on drying time when the drying time is more than 2 wk. Possible other explanations include observations of the crack network not being as vertically oriented after many sealing cycles, thus inhibiting water from reaching lower horizons; or complete surface sealing takes place at roughly equal times.

At the cessation of the rainstorm, evaporation begins from the surface and redistribution continues, both vertically and horizontally, away from the initial cracks. The drying and subsequent shrinkage of the soil at the surface eventually builds up enough stress to produce cracks (Chertkov, 2000). Not surprisingly, the preferential wetting, due to the initial cracks, leads to a nonuniform water distribution during drying and preferential formation of the subsequent cracks.

Consider the formation of the cracks after the second rainstorm (Fig. 4). The crack pattern before the second rainstorm (Fig. 3) is a prominent feature in the crack pattern following the second rainstorm (Fig. 4). The initial cracks in Fig. 3 have become low spots that have not cracked in Fig. 4, but more importantly, the initial centers of the prismatic columns (Fig. 3) have become the vertices of the subsequent cracks (Fig. 4). This is somewhat surprising, as many previous field studies have observed the cracks to return to their initial positions after a rainstorm (White, 1972; Waller and Wallender, 1993).

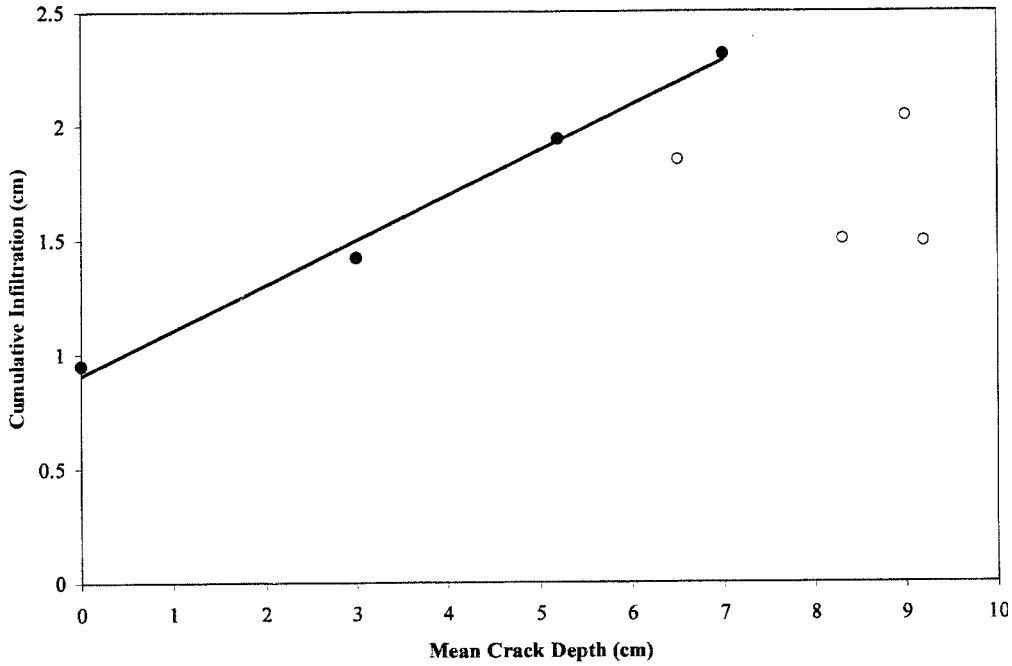

Fig. 8. Cumulative infiltration through eight rainstorms plotted as a function of the average crack depth before the onset of the rainstorm. The solid circles are the first four rainstorm data points and the open circles are the last four. The linear fit was based on the first four rainstorms.

The pattern alternates or appears to deviate from a repetition of the previous pattern due, in part, to the wetting front position. The elevation maps and the penetrometer results show that the previous centers of the prismatic columns are the highest vertically, and are surrounded by the least amount of water. Meanwhile, the previous cracks are the lowest vertically and are surrounded by the most amount of water. Thus, we see that the first cracks originate from the first part of the surface to dry. The exact mechanism is unclear as to why the cracks originate from the driest portions (the drier the soil, the greater the shrinkage, and quite probably the greater the stress, although the resistance to fracture is greater at lower water contents [Murdoch, 1993]). In any case, once the initial cracks form they grow quickly and dominate the cracking pattern.

The difference between an alternating crack pattern and a recurring crack pattern has a great impact on the preferential flow characteristics of the soil. In a recurring crack pattern the water will continue to infiltrate into specific areas of the soil (i.e., the crack positions) thus bypassing much of the soil. In an alternating crack pattern the water will not bypass nearly as much, and the overall wetting with time will be more uniform.

It is clear that the large heterogeneity in water contents and soil surface position after the second rainfall dominates where the next cracks form. After the first rainstorm, the soil surface and wetting front depth shows very minor heterogeneity. But surprisingly, this small amount of heterogeneity (or fluctuations) can easily get magnified into the large cracks that are observed. This can be seen in a close examination of the elevation maps taken immediately following the first rainstorm (Fig. 2) and after 9 d of drying (Fig. 3). The elevation map of the soil surface, immediately following the rainstorm, reveals several high and low elevation points between 0.4 and 0.6 cm. For example, focus on a ridge of high elevation measurements that begin on the *x*-axis above the 40-cm tick (Fig. 2). The high elevations move parallel to the *y*-axis to 12 cm, then branch right and left. The left branch continues vertically to the right until 24 cm, and then turns back to the left. This pattern is clearly visible in Fig. 3 as well. Thus, even changes in drying at a small scale may be magnified into determining the cracking pattern. Here, the high elevations are playing a noticeable role in the development of the cracking pattern.

CONCLUSIONS

Cumulative infiltration measurements, water position measurements, and surface geometry changes over time were presented from two experiments using simulated rainfall and an expansive clay soil. For the first four rainstorms/drying cycles, cumulative infiltration increased linearly with the crack depth; however, this relationship did not continue for subsequent storms. Near the cracks, the wetting front depth was greatest and increased with each rainstorm/drying cycle. Near the centers of the prismatic columns, the wetting front depth was smallest and decreased with each rainstorm/drying cycle. Importantly, the cracks did not reappear in the same position from rainstorm to rainstorm, instead the cracking pattern was observed to alternate between subsequent rainstorms. We interpret this to occur, due in large part to the variations in water position after the rainstorm. The combination of these results leads to a more uniform wetting at depth as time increases and the number of rainstorms increases, thereby reducing the extent of preferential flow. We are continuing simi-

lar work with intact columns taken from the same field site.

REFERENCES

Baumhardt, R.L., M.J.M. Römkens, F.D. Whisler, and J.-Y. Parlange. 1990. Modeling infiltration into a sealing soil. Water Resour. Res. 26:2497–2505.

Bonsu, M. 1992. A physically based model for surface sealing of soil. J. Soil Sci. 43:229–235.

Bronswijk, J.J.B. 1991. Drying, cracking, and subsidence of a clay soil in a lysimeter. Soil Sci. 152:92–99.

Chertkov, V.Y. 2000. Using surface crack spacing to predict crack network geometry in swelling soils. Soil Sci. Soc. Am. J. 64:1918–1921.

Chertkov, V.Y., and I. Ravina. 1998. Modeling the crack network of swelling clay soils. Soil Sci. Soc. Am. J. 62:1162–1171.

Dasog, G.S., D.F. Acton, A.R. Mermut, and E. De Jong. 1988. Shrink-swell potential and cracking in clay soils of Saskatchewan. Can. J. Soil Sci. 68:251–260.

El Abedine, Z., and G.H. Robinson. 1971. A study on cracking in some Vertisols of Sudan. Geoderma 5:229–241.

Germann, P.F., and K. Beven. 1982. Macropores and water flow in soils. Water Resour. Res. 18:1311–1325.

Haines, W.B. 1923. The volume changes associated with variations of water content in soils. J. Agric. Sci. 13:296–311.

Johnston, J.R., and H.O. Hill. 1944. A study of the shrinking and swelling properties of Rendzina soils. Soil Sci. Soc. Am. Proc. 9:24–29.

Meyer, L.D. 1958. An investigation of methods for simulating rainfall on standard runoff plots and a study of the drop size, velocity, and kinetic energy of selected spray nozzles. Special Report No. 81, Eastern Soil and Water Conservation Research Branch, Agricultural Research Service, USDA, Lafayette, IN.

Mualem, Y., and S. Assouline. 1989. Modeling soil seal as a nonuniform layer. Water Resour. Res. 25:2101–2108.

Murdoch, L.C. 1993. Hydraulic fracturing of soil during laboratory experiments. Part 2. Propagation. Geotechnique 43:267–276.

Parlange, J.-Y., W.L. Hogarth, and M.B. Parlange. 1984. Optimal analysis of the effect of a surface crust. Soil Sci. Soc. Am. J. 48:494–497.

Philip, J.R. 1969. Hydrostatics and hydrodynamics in swelling soils. Water Resour. Res. 5:1070–1077.

Philip, J.R. 1998. Infiltration into crusted soils. Water Resour. Res. 34:1919–1927.

Römkens, M.J.M., S. Singarayar, and C.J. Gantzer. 1986a. An automated non-contact surface profile meter. Soil Tillage Res. 6:193–202.

Römkens, M.J.M., J.Y. Wang, and R.W. Darden. 1988. A laser microreliefmeter. Trans. ASAE 31:408–413.

Römkens, M.J.M., R.L. Baumhardt, M.B. Parlange, F.D. Whisler, J.-Y. Parlange, and S.N. Prasad. 1986b. Rain-induced surface seals: Their effect on ponding and infiltration. Ann. Geophys. 4:417–424.

Smiles, D.E. 1974. Infiltration into a swelling material. Soil Sci. 117:140–147.

Smith, R.E., C. Corradini, and F. Melone. 1999. A conceptual model for infiltration and redistribution in crusted soils. Water Resour. Res. 35:1385–1393.

Tackett, J.L., and R.W. Pearson. 1965. Some characteristics of soil crusts formed by simulated rainfall. Soil Sci. 99:407–413.

Waller, P.M., and W.W. Wallender. 1993. Changes in cracking, water content, and bulk density of salinized swelling clay field soils. Soil Sci. 156:414–423.

White, E.M. 1970. Giant desiccation cracks in central South Dakota soils. Soil Sci. 110:71–73.

White, E.M. 1972. Soil-desiccation features in South Dakota depressions. J. Geol. 80:106–111.

White, E.M. 2001. Comments on "Using surface crack spacing to predict crack network geometry in swelling soils." Soil Sci. Soc. Am. J. 65:1573–1574.